

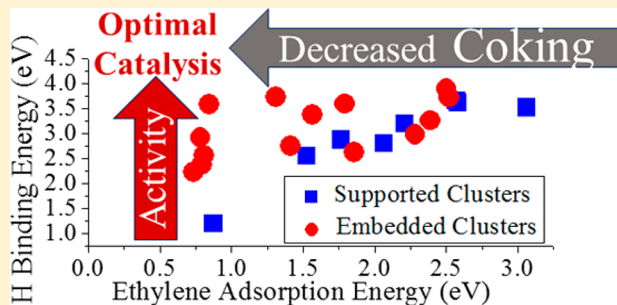
Effect of Embedding Platinum Clusters in Alumina on Sintering, Coking, and Activity

Arthur C. Reber^{ID} and Shiv N. Khanna^{*ID}

Department of Physics, Virginia Commonwealth University, Richmond, Virginia 23284, United States

S Supporting Information

ABSTRACT: First-principles theoretical studies of Pt_n ($n = 1\text{--}7$) clusters supported on pristine $\alpha\text{-Al}_2\text{O}_3$ (0001) and embedded in vacancies in the alumina surface have been carried out to investigate the effect of embedding and overcoating on coking, sintering, and catalytic activity. The hydrogen adsorption energy and the ethylene adsorption energy are used as proxies for estimating the cluster's relative activity for C–H bond activation and coking. The embedded clusters are found to exhibit enhanced stability, indicating that they are less prone to sintering. The hydrogen and ethylene adsorption energy of platinum clusters supported on pristine $\alpha\text{-Al}_2\text{O}_3$ are found to be correlated, suggesting that an increase in activity will also cause an increase in coking. Embedded clusters offer a pathway to maintain the catalytic activity while reducing the coking. Embedding the clusters makes the platinum more negatively charged, which repels ethylene, minimizing a critical pathway that leads to coking. The studies provide microscopic insight into the reduced coking in overcoated catalysts and offer a pathway toward reducing coking and sintering while maintaining the activity of the catalyst.



1. INTRODUCTION

Transition metal nanoparticles supported on metal oxide supports have been used as heterogeneous catalysts for a variety of catalytic applications including oxidation reactions and activation of hydrocarbons.^{1–12} Two of the major mechanisms that deactivate a nanoparticle catalyst are sintering of the nanoparticles and coking. Sintering of the small clusters results in larger particles that reduce the surface area of the metal and negates the unique properties of the nanoparticles.^{13–18} Coking reduces the activity of the catalyst by coating the metal particle with carbon or other intermediates that block the active sites.^{19–22} Thus one of the major challenges in developing nanoparticle catalysts is identifying and understanding strategies for minimizing coking and sintering while maintaining the activity.

One approach for preventing sintering involves embedding the cluster in an oxide layer of alumina, silica, tin oxide, or ceria.^{1,23–28} These embeddings may be carried out using chemical vapor deposition, through impregnation, or by chemically depositing an overcoating oxide layer.^{29–37} A related strategy is to induce defects into the structure of the support, and the defects may serve as anchoring sites to reduce sintering.^{38–53} For the reduction of coking, especially for reactions involving hydrocarbons, one approach is to passivate the active sites with traces of tin, boron, gallium, or other trace metals,^{54–59} which is also likely to reduce the number of active sites and potentially may deactivate catalyst. There is therefore a considerable interest in finding ways in which one could simultaneously reduce sintering and coking without adversely affecting the catalytic activity.

The overcoating of transition-metal clusters and nanoparticles has been proposed to reduce both sintering and coking.¹ Lu et al. performed a study focusing on Pd nanoparticles supported on Al_2O_3 for the activation of hydrocarbons. They showed that an alumina (Al_2O_3) overcoating of the Pd nanoparticles can reduce sintering while simultaneously reducing coking, even for high-temperature applications. They examined the oxidative dehydrogenation of ethane to ethylene, and their investigations showed that for a catalyst used for an hour at 650 °C, the amount of coke was <6%. Furthermore, a scanning electron microscopy of the sample showed no changes in the morphology even for reactions lasting up to 28 h. These are remarkable findings as the catalyst also showed improved activity compared with other approaches.

The purpose of this paper is to carry out theoretical studies of the stability and electronic structure of small Pt_n clusters supported and embedded in an $\alpha\text{-Al}_2\text{O}_3$ substrate. Our first objective is to examine how the embedding affects the adsorption energy of the cluster compared with supported species and how it varies with the size of the cluster. This requires an extensive search of the size-dependent structure of platinum clusters on pristine α -alumina and embedded in alumina with Al_4O_6 and Al_8O_{12} vacancies. We also examine the energy required to remove a single Pt atom from the supported or embedded species. Both of these energies are indicative of

Received: July 27, 2017

Revised: September 6, 2017

Published: September 15, 2017

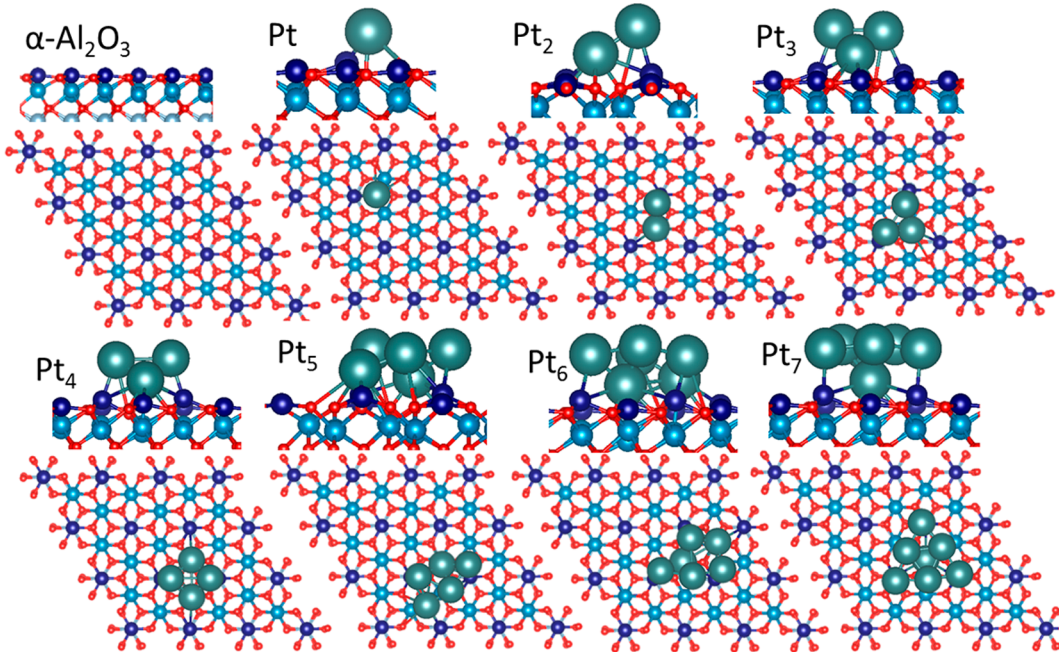


Figure 1. Structure of $\alpha\text{-Al}_2\text{O}_3$ (0001) and Pt_n , $n = 1\text{--}7$ on pristine $\alpha\text{-Al}_2\text{O}_3$ (0001).

the resistance to sintering. We are interested in examining how embedding affects the catalytic activity. For this portion, we chose the oxidation of ethane as the test reaction. Instead of examining the reaction barrier we focus on two parameters that govern the process. To this end, we calculated the adsorption energy of a hydrogen atom as the C–H activation is critical to the activity of the embedded cluster, and the hydrogen binding is a good indicator of the cluster's ability to activate the C–H bond. We also examine the adsorption energy of ethylene, a critical intermediate in the coking process. A higher binding of ethylene to the catalyst indicates that desaturated hydrocarbons will stick to the cluster, leading to coking, whereas a weak binding of ethylene makes it more likely that the product will leave the catalyst, thus reducing the poisoning of the active sites. Our objective here is to provide a qualitative insight into the factors controlling the reactivity and coking of the supported and embedded species.

2. COMPUTATIONAL APPROACH

Present theoretical studies are based on the dispersion corrected relativistic density functional theory (DFT) within the generalized gradient approximation (GGA) proposed by Perdew, Burke, and Ernzerhof (PBE) for the exchange and correlation functional⁶⁰ while using DFT-D2 to include the van der Waals corrections.⁶¹ The inclusion of relativistic corrections is important as Pt is a heavy metal. The actual computations are performed using the VASP code.^{62,63} In this work, we focused on Pt clusters containing up to seven atoms. The support was modeled by taking a periodic cell of 72 Al atoms and 108 O atoms in the structure of $\alpha\text{-Al}_2\text{O}_3$. For the embedded clusters, part of the Al and O sites at the surface was removed to accommodate the cluster. The binding energy of the cluster, E_{cluster} was calculated using the expression

$$\begin{aligned} E_{\text{cluster}} &= E(\text{support}) + E(\text{cluster}) \\ &\quad - E(\text{support} + \text{supported/embedded cluster}) \end{aligned} \quad (1)$$

The binding energy of Pt, E_{Pt} was calculated using the expression

$$E_{\text{Pt}} = E(\text{Pt}_{n-1} + \text{support}) + E(\text{Pt}) - E(\text{Pt}_n + \text{support}) \quad (2)$$

The adsorption energy of the H and ethylene to the supported and embedded clusters was calculated using similar expressions. Note that the H adsorption energy is the binding energy of a hydrogen atom and not a H_2 molecule. The geometry optimization of the cluster supported or embedded in the surface was performed with the bottom two layers of the alumina support fixed, while the top three layers were free to relax.

RESULTS AND DISCUSSION

Theoretical studies began with the ground-state structures of the Pt_n clusters supported on pristine $\alpha\text{-Al}_2\text{O}_3$ (0001). Figure 1 shows the ground-state structures for pristine Al_2O_3 , along with clusters containing up to seven atoms. The color scheme uses dark blue for the terminal Al atoms, teal for the first sublayer of Al atoms, light blue for the deeper Al atoms, and dark teal for the larger Pt atoms. As opposed to bulk Pt, which is nonmagnetic, the Pt_2 and Pt_7 clusters have ground-state structures with a spin magnetic moment of $2 \mu_B$. It is interesting to note that the spin magnetic moment in small clusters is not unique to Pt. Our previous studies had indicated ferromagnetic character in small Rh_n and Pd_n clusters that was later confirmed by Stern-Gerlach experiments in beams.^{64,65} Pt_7 is found to be the first cluster that has a bilayer structure, whereas Pt_n , $n = 1\text{--}6$, all have monolayer structures, similar to what was found in previous studies of transition-metal clusters on $\alpha\text{-Al}_2\text{O}_3$ (0001).^{57,66\text{--}70} A single Pt atom is found to bind preferentially near the terminal Al atom, with the second Pt atom binding above a subsurface Al atom. This pattern is maintained until we reach Pt_7 , when the cluster forms a planar Pt_6 motif, where each edge Pt binds to a terminal Al atom, while the seventh sits below the Pt_6 atom plane and sits above a subsurface Al atom. Platinum clusters have a strong tendency

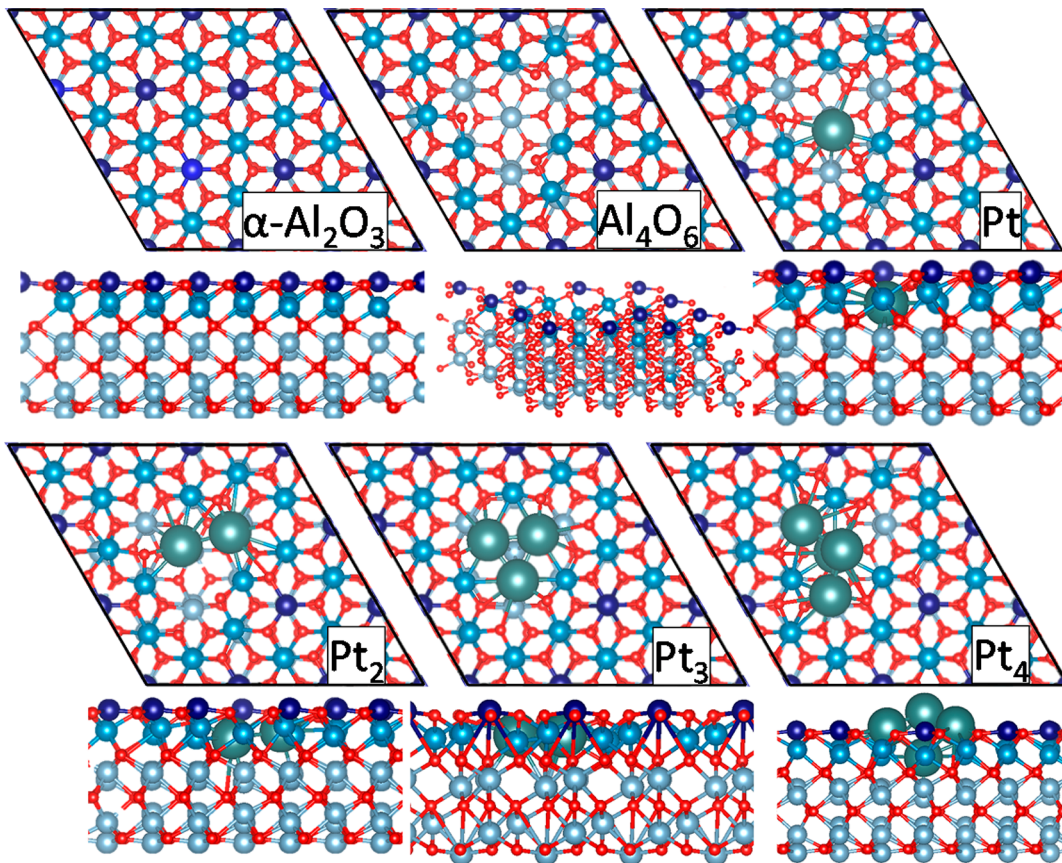


Figure 2. Structure of $\alpha\text{-Al}_2\text{O}_3$ (0001), with an Al_4O_6 void, and Pt_n , $n = 1–4$, on $\alpha\text{-Al}_2\text{O}_3$ (0001) with an Al_4O_6 void.

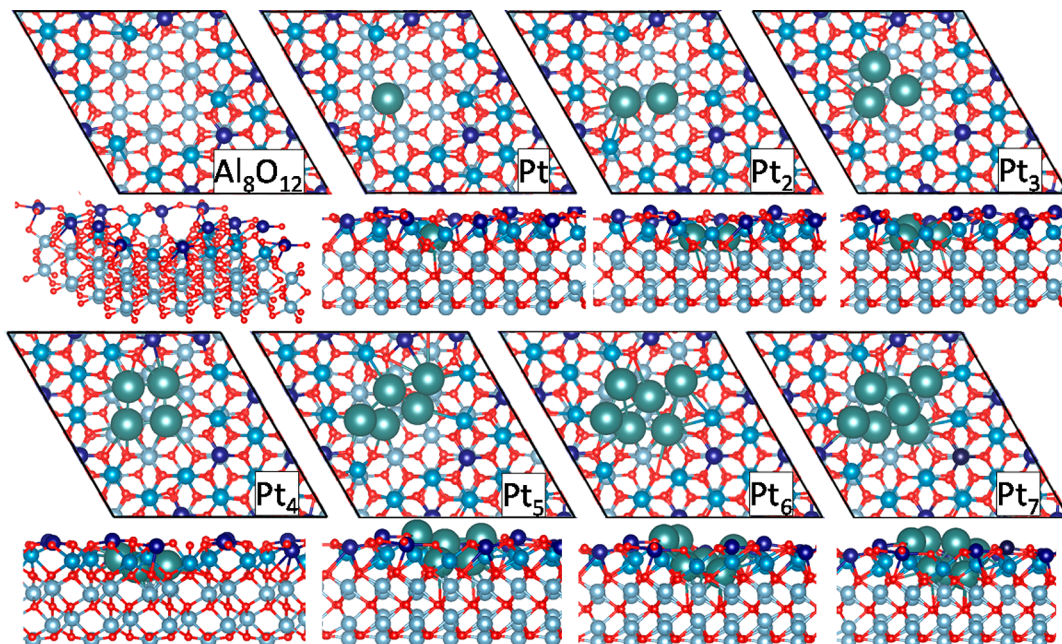


Figure 3. Structure of $\alpha\text{-Al}_2\text{O}_3$ (0001) with an Al_8O_{12} void and Pt_n , $n = 1–7$, on $\alpha\text{-Al}_2\text{O}_3$ (0001) with an Al_8O_{12} void.

toward planar structures,^{71–73} so the Pt_7 structure with the planar Pt_6 motif is found to be the ground state.

Our objective in this paper is to focus on the effect of embedding platinum clusters in Al_2O_3 . To model this, we removed four Al atoms and six O atoms to form a large void within the alumina support, as seen in Figure 2. Here the most

stable void removes three terminal Al, and one subsurface Al atoms, with the remaining O atoms bridging the remaining Al sites. The Al_2O_3 surface was modeled as a five-layer slab with the bottom two layers being fixed in the position of bulk, whereas the top three layers are free to optimize. This void energy is 26.8 eV, which is consistent with losing nine Al–O

bonds by removing the Al_4O_6 cluster. Figure 2 shows the structures of the clusters with the Al_4O_6 void. The first Pt atom binds close to the center of the void, binding to three bridging O atoms from one side of the void and a second Pt–O bond from the opposite side of the void. The addition of a second Pt atom leads to one atom sitting above an exposed subsurface Al atom and the second binding to a similar site as the first Pt atom. The Pt trimer leads to a structure in which the Pt atoms fill the void and sit above the three subsurface Al atoms. This is the largest cluster in which all three atoms fit within the Al_4O_6 void. The Pt_4 cluster is found to have a most stable structure when the cluster is turned on its side, with the fourth Pt atom lying above the void and bound only to the other Pt atoms. Because of the small size of the void, we did not consider clusters larger than Pt_4 .

Figure 3 shows the structures of the Pt_n clusters embedded within an Al_8O_{12} void. The void in the α -alumina removes three terminal Al atoms and five subsurface Al Atoms. The Pt atom in the Al_8O_{12} void bridges two subsurface Al atoms, and the Pt_2 cluster adds a second Pt atom that sits above a second triangle of subsurface Al atoms. Pt_3 is found to form a structure with the third atom binding to the exposed O atoms on the edge of the void, and Pt_4 has a pseudoplanar structure within the void. Pt_5 in the Al_8O_{12} void has a half-bowl structure with two Pt atoms sitting at the bottom of the void and the three Pt atoms sitting on the edge of the void. Pt_6 also has a bowl-like structure with three Pt atoms at the bottom of the void and the three Pt atoms along the edge of the void. Pt_7 is found to have a bilayer structure that is similar to that of Pt_6 except that a Pt atom is added on top of the deeply bound Pt.

Next, we examine how the embedding of the Pt clusters affects the stability of the clusters. Figure 4 plots the binding

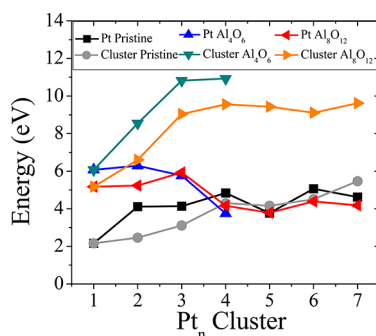


Figure 4. Pt atom binding energy and cluster binding energy of Pt_n clusters, $n = 1-7$, on pristine $\alpha\text{-Al}_2\text{O}_3$ (0001), $n = 1-4$, on alumina with an Al_4O_6 void, and $n = 1-7$ on alumina with an Al_8O_{12} void.

energy of the cluster to the support and the Pt removal energy for Pt_n , $n = 1-7$, on pristine alumina, Pt_n , $n = 1-4$, on the Al_4O_6 void, and Pt_n , $n = 1-7$, on the Al_8O_{12} void. The cluster binding energies of the embedded clusters are significantly higher than those on pristine Al_2O_3 . The binding of a single Pt atom to the Al_4O_6 and Al_8O_{12} void is 5.18 and 6.07 eV, respectively, whereas the single Pt atom binds to pristine alumina binds with 2.16 eV of energy. The cluster binding energy increases to 10.93 eV for Pt_4 in the Al_4O_6 void and 9.56 eV for Pt_4 in the Al_8O_{12} void. The Pt binding energy is significantly larger for Pt_n , $n = 1-3$, in both the Al_4O_6 and Al_8O_{12} voids, whereas for $n = 4-7$, the Pt binding energies for the embedded clusters are similar to those on pristine alumina. The increased cluster binding energy and increased Pt binding

energy indicate that embedding significantly increases the stability of small clusters in vacancies in alumina.

We next examine the effect of embedding on the electronic structure of the platinum clusters. Pt clusters on α -alumina (0001) are typically negatively charged as the terminal Al atoms may donate charge to the supported clusters. The embedded Pt atoms are even more negatively charged than on pristine alumina. As seen in Figure 5, the charge on a Pt atom on

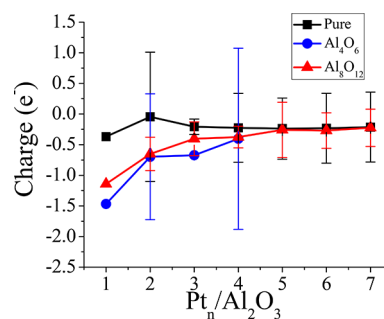


Figure 5. Average Bader charge and standard deviation of the atomic charges of Pt_n clusters, $n = 1-7$ on pure $\alpha\text{-Al}_2\text{O}_3$ (0001), $n = 1-4$ on alumina with an Al_4O_6 void, and $n = 1-7$ on alumina with an Al_8O_{12} void.

pristine alumina is -0.37 e^- , whereas it is -1.47 e^- and -1.14 e^- on the Al_4O_6 and Al_8O_{12} vacancies. The increased charge transfer to the platinum is due to the void, resulting in some Al atoms with fewer Al–O bonds that add defect-like filled states into the band gap that may then transfer charge to the platinum. The average charge donation to the embedded clusters decreases with cluster size, and by Pt_5 the charge on the embedded platinum clusters is similar to those on pristine alumina. The bars in Figure 5 indicate the standard deviation of the atomic Bader charges, showing that there may be significant variation in the charge on the cluster, depending on the position of the atoms. For example, for a Pt_4 in the Al_4O_6 void, the charge on the subsurface Pt atom is -2.57 e^- , whereas the Pt atom that lies above the surface is -0.13 e^- . This result is a bit surprising as the dangling oxygen atoms may be expected to extract charge from the platinum cluster; however, the oxygen atoms in the support are all at least doubly bonded to Al, and that Al donates charge much more effectively than Pt. The result of this is that the charge on the Pt clusters become more negatively charged inside of the defect.

We next investigate the hydrogen atom adsorption energy and the ethylene adsorption energies to the platinum clusters. Note that we are showing the adsorption energy of a hydrogen atom and that the corresponding atomic binding energy in H_2 corresponds to 2.26 eV. This means that all H atoms with adsorption energies larger than 2.26 eV are thermodynamically more stable bound to metal than as H_2 . An increase in the adsorption energy of the H atom is a signature of the enhancement in catalytic activity, and the increase in the binding energy of ethylene is a sign of the increase in coking. In Figure S1 we have plotted the hydrogen adsorption energies and the ethylene adsorption energies as a function of size defect. Figure 6 shows the hydrogen adsorption energy versus the ethylene adsorption energy. On pristine alumina, Pt_{1-3} are found to bind H most strongly, with a decrease at larger sizes. We suspect that the high adsorption energy of the H atom to the smaller Pt clusters is due to the d-band center of clusters. Figure S2 shows the 5d-band center with respect to the Fermi

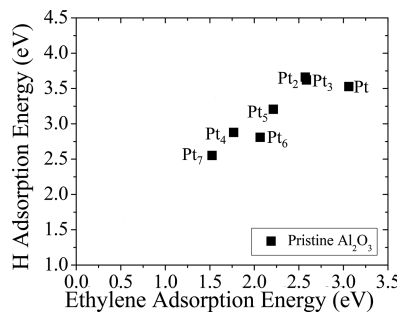


Figure 6. Hydrogen atom adsorption energy and ethylene adsorption energy on Pt_n clusters, $n = 1–7$, on pure $\alpha\text{-Al}_2\text{O}_3$ (0001).

energy, and the highest 5d-band centers are for Pt, Pt_2 , and Pt_3 respectively. When we examine the hydrogen and ethylene adsorption energies on pristine alumina in Figure 6, we find that an increase in hydrogen adsorption energy is also accompanied by an increase in the ethylene adsorption energy. This indicates that for supported species any increase in catalytic activity also leads to increased coking. This is undesirable and raises the question of whether the trend can be changed by embedding the clusters.

Figure 7 shows that embedding the clusters leads to variations in H and ethylene binding that are not correlated.

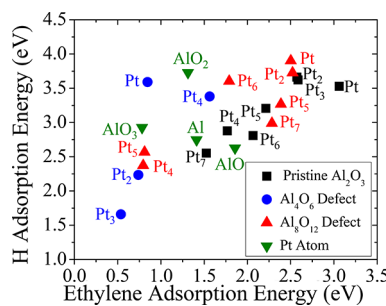


Figure 7. Hydrogen atom adsorption energy and ethylene adsorption energy on Pt_n clusters, $n = 1–7$, on pure $\alpha\text{-Al}_2\text{O}_3$ (0001), $n = 1–4$ on alumina with an Al_4O_6 void, and $n = 1–7$ on alumina with an Al_8O_{12} void, and Pt on an AlO_n void, $n = 0–3$.

For example, a Pt atom in the Al_4O_6 void has a H atom adsorption energy of 3.59 eV and an ethylene adsorption energy of 0.78 eV, while a Pt atom on pristine alumina has a H atom adsorption energy of 3.53 eV and an ethylene adsorption energy of 3.06 eV. This shows that embedding an atom reduces the ethylene adsorption energy while maintaining the atoms affinity for hydrogen. Other examples include Pt_6 in an Al_8O_{12} void, which has a H adsorption energy of 3.60 eV with an ethylene adsorption energy of 1.79 eV versus 2.81 and 2.06 eV on pristine alumina, and Pt_4 in a Al_4O_6 void, whose adsorption energies are 3.38 and 1.56 eV versus 2.88 and 1.77 eV on pristine alumina. Nine of the 11 embedded clusters have lower ethylene adsorption energies than on the corresponding cluster supported on pristine alumina. The major counterexample is Pt_7 , which has an adsorption energy on pristine Al_2O_3 of 1.53 eV and an ethylene adsorption energy of 2.28 eV in the Al_8O_{12} void. Pt_7 on pristine alumina has a unique, highly symmetric triangular structure. The reactivity and adsorption energies of clusters are often minimized by highly symmetric structures that result in an even charge distribution, while asymmetric structures with adatoms and vacancies often lead to an uneven

charge distribution and enhanced reactivity.^{74,75} For this reason, the ethylene adsorption energy to Pt_7 is unusually low, whereas Pt_7 on in an Al_8O_{12} void has low symmetry and adatom like defects that will increase ethylene binding. By examining the results, we see that the range of ethylene adsorption energies is significantly reduced by embedding the clusters. The embedded clusters offer further evidence that the 5d-band center is responsible for the H binding energy. $\text{Pt}_{1–2}$ on an Al_8O_{12} void and Pt and Pt_4 on the Al_4O_6 void have the highest 5d-band centers (Figure S2) in each of the series, and they both have the highest H binding energies in their respective series. Furthermore, Pt_6 on a Al_8O_{12} void has an relatively high 5d-band center, and it has the third highest H adsorption energy in the Al_8O_{12} void series. We find that the higher the 5d-band center, the more strongly the H binds, as the high-lying 5d-band center reduces the antibonding hydrogen–transition-metal interactions. We note that comparing the 5d-band centers between the different series does not work very well in predicting the H adsorption energies, but within a given series the 5d-band center accurately predicts the relative H adsorption energy. These results indicate that it is indeed possible to simultaneously attain high reactivity and low coking by embedding the catalytic species.

To probe the microscopic origin of the variation in the ethylene adsorption energy, we next consider the case of a single Pt site supported on the surface and embedded in a hole created by an Al atom and zero to three oxygen atoms. The more oxygen atoms that are bound to the Pt atom, the more charge is pulled from the platinum atom. In other words, if the void has a larger ratio of Al atoms, then the platinum should be positively charged, whereas if the void has a larger number of O atoms, then the platinum should be more negatively charged. Figure 8 shows the ethylene adsorption energy and the Bader

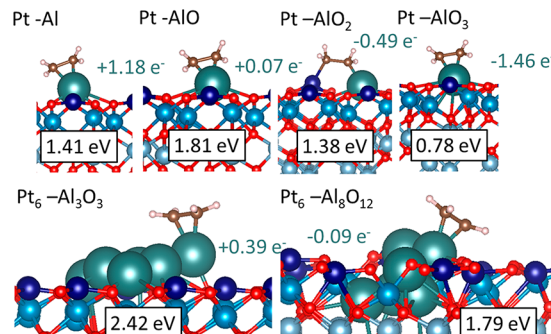


Figure 8. Ethylene adsorption energy and local Pt charges on Pt on an Al and AlO_n , $n = 1–3$, defect and Pt_6 clusters on an Al_3O_3 and Al_8O_{12} defect.

charges of the Pt atom. The AlO_3 void has the most negatively charged Pt atom and the more weakly bound ethylene, whereas Pt-AlO has the most strongly bound ethylene. The lone pair of ethylene is expected to interact with the Pt atom, so the more positive the platinum, the more strongly it is expected to bind the ethylene. The correlation between charge and ethylene binding does not predict that the Pt in an Al vacancy binds ethylene more weakly than the AlO void. We have also investigated the effect of void on Pt_6 cluster in an Al_3O_3 and Al_8O_{12} void. As seen in Figure 8, Pt_6 on Al_3O_3 is more positive and more strongly binds ethylene, whereas in the case of Pt_6 on an Al_8O_{12} void the ethylene adsorption energy is weaker with a more negative charge. This analysis reveals that by making the

Pt more negative the interaction with ethylene becomes weaker and hence the primary intermediate that leads to coking is diminished. Charging the Pt clusters through embedding does not reduce the activity of the cluster, whereas it does reduce the ethylene adsorption energy. These results help to explain why clusters that are embedded in alumina not only have reduced sintering but also have reduced coking. Furthermore, if the stoichiometry of the vacancies may be controlled, this offers a strategy for reducing coking while maintaining catalyst activity.

4. CONCLUSIONS

To summarize, the present studies suggest a viable pathway to designing catalysts that can offer reduced sintering and coking while maintaining the activity. We have shown that embedding the Pt_n clusters in holes created on the surface can lead to stable species that have enhanced stability and are less prone to sintering. The platinum clusters experience a charge flow from the support to the Platinum clusters. For clusters supported on the pristine surface, the amount of the charge flow is small. However, embedding the clusters in defects enhances the charge flow, and this charge flow may be further tuned by changing the composition of the void on the surface. The adsorption energy of the ethylene decreases as the charge on the platinum becomes more negative, offering an additional strategy for decreasing the coking of the catalyst. We find that the activity of the supported and embedded clusters may be rationalized though the 5d-band centers and that embedding does not reduce the activity of the clusters. These findings offer a microscopic insight by which the activity of an embedded cluster may be maintained while reducing sintering and coking.

■ ASSOCIATED CONTENT

S Supporting Information

The Supporting Information is available free of charge on the ACS Publications website at DOI: [10.1021/acs.jpcc.7b07452](https://doi.org/10.1021/acs.jpcc.7b07452).

H and ethylene adsorption energies and 5d band centers.
(PDF)

■ AUTHOR INFORMATION

Corresponding Author

*E-mail: snkhanna@vcu.edu. Tel/Fax: +1 804-828-1820/+1 804-828-7073.

ORCID

Arthur C. Reber: [0000-0003-1013-331X](https://orcid.org/0000-0003-1013-331X)

Shiv N. Khanna: [0000-0002-9797-1289](https://orcid.org/0000-0002-9797-1289)

Author Contributions

The manuscript was written through contributions of all authors. All authors have given approval to the final version of the manuscript.

Notes

The authors declare no competing financial interest.

■ ACKNOWLEDGMENTS

This material is based on work supported by the U.S. Department of Energy (DOE) under the award number DE-SC0006420.

■ REFERENCES

- (1) Lu, J.; Fu, B.; Kung, M. C.; Xiao, G.; Elam, J. W.; Kung, H. H.; Stair, P. C. Coking- and Sintering-Resistant Palladium Catalysts Achieved Through Atomic Layer Deposition. *Science* **2012**, *335*, 1205–1208.
- (2) Lee, S.; Lee, B.; Mahmood, F.; Seifert, S.; Libera, J. A.; Elam, J. W.; Greeley, J.; Zapol, P.; Curtiss, L. A.; Pellin, M. J.; et al. Oxidative Decomposition of Methanol on Subnanometer Palladium Clusters: The Effect of Catalyst Size and Support Composition. *J. Phys. Chem. C* **2010**, *114*, 10342–10348.
- (3) Vajda, S.; Pellin, M. J.; Greeley, J. P.; Marshall, C. L.; Curtiss, L. A.; Ballantine, G. A.; Elam, J. W.; Catillon-Mucherrie, S.; Redfern, P. C.; Mahmood, F.; et al. Subnanometre Platinum Clusters as Highly Active and Selective Catalysts for the Oxidative Dehydrogenation of Propane. *Nat. Mater.* **2009**, *8*, 213–216.
- (4) Kwon, G.; Ferguson, G. A.; Heard, C. J.; Tyo, E. C.; Yin, C.; DeBartolo, J.; Seifert, S.; Winans, R. E.; Kropf, A. J.; Greeley, J.; et al. Size-Dependent Subnanometer Pd Cluster (Pd_4 , Pd_6 , and Pd_{17}) Water Oxidation Electrocatalysis. *ACS Nano* **2013**, *7*, 5808–5817.
- (5) Kaden, W. E.; Wu, T.; Kunkel, W. A.; Anderson, S. L. Electronic Structure Controls Reactivity of Size-Selected Pd Clusters Adsorbed on TiO_2 Surfaces. *Science* **2009**, *326*, 826–829.
- (6) Kaden, W. E.; Kunkel, W. A.; Kane, M. D.; Roberts, F. S.; Anderson, S. L. Size-Dependent Oxygen Activation Efficiency over $\text{Pd}_n/\text{TiO}_2(110)$ for the CO Oxidation Reaction. *J. Am. Chem. Soc.* **2010**, *132*, 13097–13099.
- (7) Rodriguez, A. A.; Williams, C. T.; Monnier, J. R. Selective Liquid-Phase Oxidation of Glycerol over Au–Pd/C Bimetallic Catalysts Prepared by Electroless Deposition. *Appl. Catal., A* **2014**, *475*, 161–168.
- (8) Zhang, Y.; Diao, W.; Williams, C. T.; Monnier, J. R. Selective Hydrogenation of Acetylene in Excess Ethylene Using Ag- and Au–Pd/ SiO_2 Bimetallic Catalysts Prepared by Electroless Deposition. *Appl. Catal., A* **2014**, *469*, 419–426.
- (9) Diao, W.; Tengco, J. M. M.; Regalbuto, J. R.; Monnier, J. R. Preparation and Characterization of Pt–Ru Bimetallic Catalysts Synthesized by Electroless Deposition Methods. *ACS Catal.* **2015**, *5*, 5123–5134.
- (10) Cai, Y. Q.; Bradshaw, A. M.; Guo, Q.; Goodman, D. W. The Size Dependence of the Electronic Structure of Pd Clusters Supported on $\text{Al}_2\text{O}_3\text{Re}(0001)$. *Surf. Sci.* **1998**, *399*, L357–L363.
- (11) Xu, C.; Oh, W. S.; Liu, G.; Kim, D. Y.; Goodman, D. W. Characterization of Metal Clusters (Pd and Au) Supported on Various Metal Oxide Surfaces (MgO and TiO_2). *J. Vac. Sci. Technol., A* **1997**, *15*, 1261–1268.
- (12) Nørskov, J. K.; Bligaard, T.; Hvolbæk, B.; Abild-Pedersen, F.; Chorkendorff, I.; Christensen, C. H. The Nature of the Active Site in Heterogeneous Metal Catalysis. *Chem. Soc. Rev.* **2008**, *37*, 2163–2171.
- (13) Harris, P. J. F. The Sintering of Platinum Particles in an Alumina-Supported Catalyst: Further Transmission Electron Microscopy Studies. *J. Catal.* **1986**, *97*, 527–542.
- (14) Nagai, Y.; Hirabayashi, T.; Dohmae, K.; Takagi, N.; Minami, T.; Shinjoh, H.; Matsumoto, S. Sintering Inhibition Mechanism of Platinum Supported on Ceria-Based Oxide and Pt-Oxide–support Interaction. *J. Catal.* **2006**, *242*, 103–109.
- (15) Nagai, Y.; Dohmae, K.; Ikeda, Y.; Takagi, N.; Hara, N.; Tanabe, T.; Guilera, G.; Pasarelli, S.; Newton, M. A.; Takahashi, N.; et al. In Situ Observation of Platinum Sintering on Ceria-Based Oxide for Autoexhaust Catalysts Using Turbo-XAS. *Catal. Today* **2011**, *175*, 133–140.
- (16) Wettergren, K.; Schweinberger, F. F.; Deiana, D.; Ridge, C. J.; Crampton, A. S.; Rötzer, M. D.; Hansen, T. W.; Zhdanov, V. P.; Heiz, U.; Langhammer, C. High Sintering Resistance of Size-Selected Platinum Cluster Catalysts by Suppressed Ostwald Ripening. *Nano Lett.* **2014**, *14*, 5803–5809.
- (17) Reber, A. C.; Khanna, S. N. Superatoms: Electronic and Geometric Effects on Reactivity. *Acc. Chem. Res.* **2017**, *50*, 255–263.
- (18) Plessow, P. N.; Sánchez-Carrera, R. S.; Li, L.; Rieger, M.; Sauer, S.; Schaefer, A.; Abild-Pedersen, F. Modeling the Interface of Platinum and α -Quartz(001): Implications for Sintering. *J. Phys. Chem. C* **2016**, *120*, 10340–10350.

- (19) Seipenbusch, M.; Binder, A. Structural Stabilization of Metal Nanoparticles by Chemical Vapor Deposition-Applied Silica Coatings. *J. Phys. Chem. C* **2009**, *113*, 20606–20610.
- (20) Barbier, J. Deactivation of Reforming Catalysts by Coking - a Review. *Appl. Catal.* **1986**, *23*, 225–243.
- (21) Kim, J.-H.; Suh, D. J.; Park, T.-J.; Kim, K.-L. Effect of Metal Particle Size on Coking during CO₂ Reforming of CH₄ over Ni-alumina Aerogel Catalysts. *Appl. Catal., A* **2000**, *197*, 191–200.
- (22) de Vekki, A. V.; Kraev, Y. L.; Solovykh, A. I. Electronic Effects in the Coke Deactivation of Platinum-Alumina Catalysts. *Pet. Chem.* **2008**, *48*, 210–218.
- (23) Alba-Rubio, A. C.; O'Neill, B. J.; Shi, F.; Akatay, C.; Canlas, C.; Li, T.; Winans, R.; Elam, J. W.; Stach, E. A.; Voyles, P. M.; et al. Pore Structure and Bifunctional Catalyst Activity of Overlayers Applied by Atomic Layer Deposition on Copper Nanoparticles. *ACS Catal.* **2014**, *4*, 1554–1557.
- (24) Yu, K.; Wu, Z.; Zhao, Q.; Li, B.; Xie, Y. High-Temperature-Stable Au@SnO₂ Core/Shell Supported Catalyst for CO Oxidation. *J. Phys. Chem. C* **2008**, *112*, 2244–2247.
- (25) Zhang, W.; Lin, X.-J.; Sun, Y.-G.; Bin, D.-S.; Cao, A.-M.; Wan, L.-J. Controlled Formation of Metal@Al₂O₃ Yolk–Shell Nanostructures with Improved Thermal Stability. *ACS Appl. Mater. Interfaces* **2015**, *7*, 27031–27034.
- (26) Mondal, K.; Sharma, A. Recent Advances in the Synthesis and Application of Photocatalytic Metal–metal Oxide Core–shell Nanoparticles for Environmental Remediation and Their Recycling Process. *RSC Adv.* **2016**, *6*, 83589–83612.
- (27) Arnal, P. M.; Comotti, M.; Schüth, F. High-Temperature-Stable Catalysts by Hollow Sphere Encapsulation. *Angew. Chem.* **2006**, *118*, 8404–8407.
- (28) Ge, J.; Zhang, Q.; Zhang, T.; Yin, Y. Core–Satellite Nanocomposite Catalysts Protected by a Porous Silica Shell: Controllable Reactivity, High Stability, and Magnetic Recyclability. *Angew. Chem.* **2008**, *120*, 9056–9060.
- (29) Liang, X.; Yu, M.; Li, J.; Jiang, Y.-B.; Weimer, W. Ultra-Thin Microporous–Mesoporous Metal Oxide Films Prepared by Molecular Layer Deposition (MLD). *Chem. Commun.* **2009**, 7140–7142.
- (30) Shang, Z.; Patel, R. L.; Evanko, W.; Liang, B. X. Encapsulation of Supported Metal Nanoparticles with an Ultra-Thin Porous Shell for Size-Selective Reactions. *Chem. Commun.* **2013**, *49*, 10067–10069.
- (31) Gould, T. D.; Izar, A.; Weimer, A. W.; Falconer, J. L.; Medlin, J. W. Stabilizing Ni Catalysts by Molecular Layer Deposition for Harsh, Dry Reforming Conditions. *ACS Catal.* **2014**, *4*, 2714–2717.
- (32) Cargnello, M.; Gentilini, C.; Montini, T.; Fonda, E.; Mehraeen, S.; Chi, M.; Herrera-Collado, M.; Browning, N. D.; Polizzi, S.; Pasquato, L.; et al. Active and Stable Embedded Au@CeO₂ Catalysts for Preferential Oxidation of CO. *Chem. Mater.* **2010**, *22*, 4335–4345.
- (33) Tong, J.; Su, L.; Haraya, K.; Suda, H. Thin Pd Membrane on α -Al₂O₃ Hollow Fiber Substrate without Any Interlayer by Electroless Plating Combined with Embedding Pd Catalyst in Polymer Template. *J. Membr. Sci.* **2008**, *310*, 93–101.
- (34) Joo, J. B.; Kim, P.; Kim, W.; Kim, J.; Yi, J. Preparation of Mesoporous Carbon Templatized by Silica Particles for Use as a Catalyst Support in Polymer Electrolyte Membrane Fuel Cells. *Catal. Today* **2006**, *111*, 171–175.
- (35) Ryoo, R.; Joo, S. H.; Jun, S. Synthesis of Highly Ordered Carbon Molecular Sieves via Template-Mediated Structural Transformation. *J. Phys. Chem. B* **1999**, *103*, 7743–7746.
- (36) Choi, K. M.; Na, K.; Somorjai, G. A.; Yaghi, O. M. Chemical Environment Control and Enhanced Catalytic Performance of Platinum Nanoparticles Embedded in Nanocrystalline Metal–Organic Frameworks. *J. Am. Chem. Soc.* **2015**, *137*, 7810–7816.
- (37) Behrens, M.; Furche, A.; Kasatkin, I.; Trunschke, A.; Busser, W.; Muhler, M.; Kniep, B.; Fischer, R.; Schlögl, R. The Potential of Microstructural Optimization in Metal/Oxide Catalysts: Higher Intrinsic Activity of Copper by Partial Embedding of Copper Nanoparticles. *ChemCatChem* **2010**, *2*, 816–818.
- (38) Sanchez, A.; Abbet, S.; Heiz, U.; Schneider, W.-D.; Häkkinen, H.; Barnett, R. N.; Landman, U. When Gold Is Not Noble: Nanoscale Gold Catalysts. *J. Phys. Chem. A* **1999**, *103*, 9573–9578.
- (39) Yang, Y.; Castano, C. E.; Gupton, B. F.; Reber, A. C.; Khanna, S. N. Fundamental Analysis of Enhanced Cross-Coupling Catalytic Activity for Palladium Clusters on Graphene Supports. *Nanoscale* **2016**, *8*, 19564–19572.
- (40) Roberts, F. S.; Anderson, S. L.; Reber, A. C.; Khanna, S. N. Initial and Final State Effects in the Ultraviolet and X-Ray Photoelectron Spectroscopy (UPS and XPS) of Size-Selected Pdn Clusters Supported on TiO₂(110). *J. Phys. Chem. C* **2015**, *119*, 6033–6046.
- (41) Reber, A. C.; Khanna, S. N. Effect of N- and P-Type Doping on the Oxygen-Binding Energy and Oxygen Spillover of Supported Palladium Clusters. *J. Phys. Chem. C* **2014**, *118*, 20306–20313.
- (42) Reber, A. C.; Khanna, S. N.; Roberts, F. S.; Anderson, S. L. Effect of O₂ and CO Exposure on the Photoelectron Spectroscopy of Size-Selected Pdn Clusters Supported on TiO₂(110). *J. Phys. Chem. C* **2016**, *120*, 2126–2138.
- (43) Haas, G.; Menck, A.; Brune, H.; Barth, J. V.; Venables, J. A.; Kern, K. Nucleation and Growth of Supported Clusters at Defect Sites: Pd/MgO(001). *Phys. Rev. B: Condens. Matter Mater. Phys.* **2000**, *61*, 11105–11108.
- (44) Zhang, J.; Alexandrova, A. N. Structure, Stability, and Mobility of Small Pd Clusters on the Stoichiometric and Defective TiO₂ (110) Surfaces. *J. Chem. Phys.* **2011**, *135*, 174702.
- (45) Goodman, D. W. Catalytically Active Au on Titania.” Yet Another Example of a Strong Metal Support Interaction (SMSI)? *Catal. Lett.* **2005**, *99*, 1–4.
- (46) Shekhar, M.; Wang, J.; Lee, W.-S.; Williams, W. D.; Kim, S. M.; Stach, E. A.; Miller, J. T.; Delgass, W. N.; Ribeiro, F. H. Size and Support Effects for the Water–Gas Shift Catalysis over Gold Nanoparticles Supported on Model Al₂O₃ and TiO₂. *J. Am. Chem. Soc.* **2012**, *134*, 4700–4708.
- (47) Kasatkin, I.; Kurr, P.; Kniep, B.; Trunschke, A.; Schlögl, R. Role of Lattice Strain and Defects in Copper Particles on the Activity of Cu/ZnO/Al₂O₃ Catalysts for Methanol Synthesis. *Angew. Chem.* **2007**, *119*, 7465–7468.
- (48) Wallace, W. T.; Min, B. K.; Goodman, D. W. The Stabilization of Supported Gold Clusters by Surface Defects. *J. Mol. Catal. A: Chem.* **2005**, *228*, 3–10.
- (49) Jenness, G. R.; Schmidt, J. R. Unraveling the Role of Metal–Support Interactions in Heterogeneous Catalysis: Oxygenate Selectivity in Fischer–Tropsch Synthesis. *ACS Catal.* **2013**, *3*, 2881–2890.
- (50) Yang, X.-F.; Wang, A.; Qiao, B.; Li, J.; Liu, J.; Zhang, T. Single-Atom Catalysts: A New Frontier in Heterogeneous Catalysis. *Acc. Chem. Res.* **2013**, *46*, 1740–1748.
- (51) Moussa, S.; Siamaki, A. R.; Gupton, B. F.; El-Shall, M. S. Pd-Partially Reduced Graphene Oxide Catalysts (Pd/PRGO): Laser Synthesis of Pd Nanoparticles Supported on PRGO Nanosheets for Carbon–Carbon Cross Coupling Reactions. *ACS Catal.* **2012**, *2*, 145–154.
- (52) Siamaki, A. R.; Khder, A. E. R. S.; Abdelsayed, V.; El-Shall, M. S.; Gupton, B. F. Microwave-Assisted Synthesis of Palladium Nanoparticles Supported on Graphene: A Highly Active and Recyclable Catalyst for Carbon–carbon Cross-Coupling Reactions. *J. Catal.* **2011**, *279*, 1–11.
- (53) Siamaki, A. R.; Lin, Y.; Woodberry, K.; Connell, J. W.; Gupton, B. F. Palladium Nanoparticles Supported on Carbon Nanotubes from Solventless Preparations: Versatile Catalysts for Ligand-Free Suzuki Cross Coupling Reactions. *J. Mater. Chem. A* **2013**, *1*, 12909–12918.
- (54) Hook, A.; Massa, J. D.; Celik, F. E. Effect of Tin Coverage on Selectivity for Ethane Dehydrogenation over Platinum–Tin Alloys. *J. Phys. Chem. C* **2016**, *120*, 27307–27318.
- (55) Yang, M.-L.; Zhu, Y.-A.; Zhou, X.-G.; Sui, Z.-J.; Chen, D. First-Principles Calculations of Propane Dehydrogenation over PtSn Catalysts. *ACS Catal.* **2012**, *2*, 1247–1258.
- (56) Gercekler, D.; Motagamwala, A. H.; Rivera-Dones, K. R.; Miller, J. B.; Huber, G. W.; Mavrikakis, M.; Dumesic, J. A. Methane

Conversion to Ethylene and Aromatics on PtSn Catalysts. *ACS Catal.* **2017**, *7*, 2088–2100.

(57) Baxter, E. T.; Ha, M.-A.; Cass, A. C.; Alexandrova, A. N.; Anderson, S. L. Ethylene Dehydrogenation on $\text{Pt}_{4,7,8}$ Clusters on Al_2O_3 : Strong Cluster Size Dependence Linked to Preferred Catalyst Morphologies. *ACS Catal.* **2017**, *7*, 3322–3335.

(58) Pham, H. N.; Sattler, J. J. H. B.; Weckhuysen, B. M.; Datye, A. K. Role of Sn in the Regeneration of $\text{Pt}/\gamma\text{-Al}_2\text{O}_3$ Light Alkane Dehydrogenation Catalysts. *ACS Catal.* **2016**, *6*, 2257–2264.

(59) Im, J.; Choi, M. Physicochemical Stabilization of Pt against Sintering for a Dehydrogenation Catalyst with High Activity, Selectivity, and Durability. *ACS Catal.* **2016**, *6*, 2819–2826.

(60) Perdew, J. P.; Burke, K.; Ernzerhof, M. Generalized Gradient Approximation Made Simple. *Phys. Rev. Lett.* **1996**, *77* (18), 3865–3868.

(61) Grimme, S. Semiempirical GGA-Type Density Functional Constructed with a Long-Range Dispersion Correction. *J. Comput. Chem.* **2006**, *27* (15), 1787–1799.

(62) Kresse, G.; Furthmüller, J. Efficient Iterative Schemes for Ab Initio Total-Energy Calculations Using a Plane-Wave Basis Set. *Phys. Rev. B: Condens. Matter Mater. Phys.* **1996**, *54*, 11169–11186.

(63) Kresse, G.; Joubert, D. From Ultrasoft Pseudopotentials to the Projector Augmented-Wave Method. *Phys. Rev. B: Condens. Matter Mater. Phys.* **1999**, *59*, 1758–1775.

(64) Khanna, S. N.; Linderoth, S. Magnetic Behavior of Clusters of Ferromagnetic Transition Metals. *Phys. Rev. Lett.* **1991**, *67*, 742–745.

(65) Cox, A. J.; Louderback, J. G.; Apsel, S. E.; Bloomfield, L. A. Magnetism in 4d-Transition Metal Clusters. *Phys. Rev. B: Condens. Matter Mater. Phys.* **1994**, *49*, 12295–12298.

(66) Nigam, S.; Majumder, C. Substrate Induced Reconstruction and Activation of Platinum Clusters: A Systematic DFT Study. *Appl. Surf. Sci.* **2017**, *422*, 1075–1081.

(67) Zhou, C.; Wu, J.; Kumar, T. J. D.; Balakrishnan, N.; Forrey, R. C.; Cheng, H. Growth Pathway of Pt Clusters on $\alpha\text{-Al}_2\text{O}_3(0001)$ Surface. *J. Phys. Chem. C* **2007**, *111*, 13786–13793.

(68) Nigam, S.; Majumder, C. Growth Pattern of Ag_n ($n = 1–8$) Clusters on the $\alpha\text{-Al}_2\text{O}_3(0001)$ Surface: A First Principles Study. *Langmuir* **2010**, *26*, 18776–18787.

(69) Nigam, S.; Majumder, C. Adsorption of Small Palladium Clusters on the $\alpha\text{-Al}_2\text{O}_3(0001)$ Surface: A First Principles Study. *J. Phys. Chem. C* **2012**, *116*, 2863–2871.

(70) Rajesh, C.; Nigam, S.; Majumder, C. The Structural and Electronic Properties of Au n Clusters on the $\alpha\text{-Al}_2\text{O}_3(0001)$ Surface: A First Principles Study. *Phys. Chem. Chem. Phys.* **2014**, *16*, 26561–26569.

(71) Chaves, A. S.; Rondina, G. G.; Piotrowski, M. J.; Tereshchuk, P.; Da Silva, J. L. F. The Role of Charge States in the Atomic Structure of Cu_n and Pt_n ($n = 2–14$ Atoms) Clusters: A DFT Investigation. *J. Phys. Chem. A* **2014**, *118*, 10813–10821.

(72) Xiao, L.; Wang, L. Structures of Platinum Clusters: Planar or Spherical? *J. Phys. Chem. A* **2004**, *108*, 8605–8614.

(73) Kumar, V.; Kawazoe, Y. Evolution of Atomic and Electronic Structure of Pt Clusters: Planar, Layered, Pyramidal, Cage, Cubic, and Octahedral Growth. *Phys. Rev. B: Condens. Matter Mater. Phys.* **2008**, *77*, 205418.

(74) Roach, P. J.; Woodward, W. H.; Castleman, A. W.; Reber, A. C.; Khanna, S. N. Complementary Active Sites Cause Size-Selective Reactivity of Aluminum Cluster Anions with Water. *Science* **2009**, *323*, 492–495.

(75) Luo, Z.; Reber, A. C.; Jia, M.; Blades, W. H.; Khanna, S. N.; Castleman, A. W. What Determines If a Ligand Activates or Passivates a Superatom Cluster? *Chem. Sci.* **2016**, *7*, 3067–3074.